Bioinspiration & Biomimetics

NOTE

Design and analysis of aerodynamic force platforms for free flight studies

Ben J Hightower[1], Rivers Ingersoll[1], Diana D Chin, Carl Lawhon, Andreas F Haselsteiner and David Lentink

Mechanical Engineering, Stanford University, Stanford, CA, United States of America
[1] Equal work.

E-mail: dlentink@stanford.edu

Abstract

We describe and explain new advancements in the design of the aerodynamic force platform, a novel instrument that can directly measure the aerodynamic forces generated by freely flying animals and robots. Such *in vivo* recordings are essential to better understand the precise aerodynamic function of flapping wings in nature, which can critically inform the design of new bioinspired robots. By designing the aerodynamic force platform to be stiff yet lightweight, the natural frequencies of all structural components can be made over five times greater than the frequencies of interest. The associated high-frequency noise can then be filtered out during post-processing to obtain accurate and precise force recordings. We illustrate these abilities by measuring the aerodynamic forces generated by a freely flying bird. The design principles can also be translated to other fluid media. This offers an opportunity to perform high-throughput, real-time, non-intrusive, and *in vivo* comparative biomechanical measurements of force generation by locomoting animals and robots. These recordings can include complex bimodal terrestrial, aquatic, and aerial behaviors, which will help advance the fields of experimental biology and bioinspired design.

Introduction

Flapping wings are nature's elegant solution to powered flight. How flying animals, such as insects, birds and bats, utilize complex wing morphologies and motions to generate aerodynamic force during free flight is still not fully understood (Shyy *et al* 2013, Chin and Lentink 2016). Our understanding is limited by a lack of *in vivo* force measurements and the reliance on indirect methods to calculate aerodynamic force.

Aerodynamic force can be calculated by integrating *in vivo* flow measurements using the control surface formulation of the Navier–Stokes equations (Noca *et al* 1999, Mohebbian and Rival 2012). The flow field is typically measured using particle image velocimetry (PIV), and then integrated to obtain the pressure field and the net force using the momentum equation (van Oudheusden 2013). Formally this requires the measurement of the velocity field over the entire control surface (Lentink *et al* 2015). In practice, these measurements are typically only made in one plane behind or below the wings (van Oudheusden 2013). Within the measurement plane, these calculations are limited by the low spatial and temporal resolution of high-speed cameras, which are unable to fully resolve turbulence (Rival and van Oudheusden 2017). Further, the algorithms required to obtain the velocity field and dependent variables suffer from numerical roundoff errors that ultimately limit the accuracy of the calculated fluid force (Lentink *et al* 2015). Other simplified quasi-steady models that were originally developed for rotorcraft and idealized vortices, such as the Kutta–Joukowski theorem (Hedenström *et al* 2006), the actuator disk model (Muijres *et al* 2011), and the vortex ring model (Johansson and Hedenström 2009), yield inconsistent results for flying animals (Gutierrez *et al* 2016). To address these limitations, direct force measurements are needed.

Forces can be measured directly by tethering animals such as insects. However, this method is inappropriate for vertebrates and yields results that do not fully generalize to maneuvering insect flight (Taylor 2001). Further, inertia forces can confound the measurement of the aerodynamic forces generated by flexible wings (Zhao *et al* 2010). The aerodynamic force platform (AFP), which we first described in Lentink *et al* (2015),

resolves these dilemmas by directly measuring the aerodynamic forces generated by freely flying animals *in vivo* as well as by robots.

The flapping wings of insects, birds and bats have inspired the development of novel flapping winged robots (e.g. Lentink *et al* 2009, Keennon *et al* 2012, Ma *et al* 2013, Ramezani *et al* 2017). However, a direct measure of the aerodynamic forces generated by these robots in free flight does not exist. Whereas robots can be tethered to estimate the average aerodynamic force (Lentink *et al* 2009), the structural vibrations of their wing confound the measurement of time-resolved aerodynamic forces via a tether (Lentink *et al* 2015). The AFP can uniquely address this in experimental setups by mechanically integrating the pressure and shear field induced by the flying animal or robot on the surfaces of a control volume away from, and not in mechanical contact with, the animal or robot. Because the AFP is non-intrusive and real-time, it enables high-accuracy measurements of undisturbed free flight maneuvers (Lentink *et al* 2015). The new method generalizes beyond flapping flight to flying vehicles, robots and aerodynamic force generation objects in general, as demonstrated by theory and validation via quadcopter (Lentink *et al* 2015).

Here we present new analysis and design principles used to develop a faster and more sensitive AFP for hummingbirds and a larger AFP to study short flights made by small generalist birds, substantially improving upon the design of our first-generation AFP. Using new aerodynamic force data for a small bird, we demonstrate for the first time how both the floor and ceiling of the control volume contribute to the total aerodynamic force measured, and how the center of pressure on each plate varies throughout a wingbeat. Finally, we explain how low frequency noise sources can be detected and mitigated, and how high-frequency noise can be attenuated using data filtering.

Methods

The AFP consists of a rigid box that integrates the pressure and shear forces on the boundaries of a control volume enclosing a freely locomoting animal or robot (figure 1(a)). The net force and moments in the control volume are recorded via instrumented contact points on a rigid supporting structure. Previously we published an analytical solution of the Navier–Stokes equations to show that this method is exact, along with an experimental validation of the AFP with a quadcopter and with freely flying birds (Lentink *et al* (2015); also summarized in supplementary information (stacks.iop.org/BB/12/064001/mmedia)).

The simplest AFP design measures vertical aerodynamic forces. We much improved upon our first-generation AFP, which was a simple box based on sandwich panels constructed out of thin balsa wood sheets with plastic covering (Lentink *et al* 2015). The new design consists of a rigid truss (80/20 aluminum

extrusions) that supports instrumented carbon fiber plates on the top and bottom that integrate the pressure field generated by flapping wings in real-time (figure 1(b)). Transparent side panels enclose the control volume and provide optical access (figure 1(c)). We implemented this design in two separate setups. The smaller setup, designed for hummingbirds (*Calypte anna*, approximate wingspan 12 cm, body mass 4.7 g, and wingbeat frequency 42 Hz) has a chamber of $0.5 \times 0.5 \times 0.5$ m and a natural frequency over 210 Hz ($\geqslant 5 \times$ wingbeat frequency), using capacitive force sensors capable of resolving 0.5 nm displacement at 10 kHz (Microsense 8800 electronics module with model 2805 probes). The large setup (for birds of wingspan up to ~50 cm, body mass up to 200 g, and wingbeat frequency up to ~20 Hz) has dimensions of $0.9 \times 1.0 \times 0.6$ m (height, width, depth) and a natural frequency greater than 100 Hz ($\geqslant 5 \times$ wingbeat frequency). Each plate is statically determined and is supported by three Nano 43 sensors (six-axis, silicon strain gage based with SI-9-0.125 calibration, ATI Industrial Automation) that sample force at 1 ms intervals with 2 mN resolution. To quantify shear forces on the sidewalls, or to measure 3D forces during more complex maneuvers, all six sides of the box must be instrumented with plates (figure 1(d) (i) and (ii)). Care must be taken when reorienting plates to minimize risk of sensor overloading. Furthermore, for measuring forces in both the normal and lateral direction, the contact point needs to be designed for sufficiently high natural frequencies in both directions. Unfortunately, using plates on all sides occludes the view of the flight arena, so we designed acrylic window ports with high natural frequencies so they do not compromise the accuracy of the measurements (figure 1(d) (iii)). Finally, to more accurately spatially resolve the pressure distribution over the entire surface of the aerodynamic control volume, arrays with multiple force plate elements must be used on all sides (figure 1(d) (iv)). All bird training and experimental procedures were approved by Stanford's Administrative Panel on Laboratory Animal Care.

Results and discussion

Optimization of the aerodynamic force platform

AFP design involves first determining the flight chamber size, developing a supporting truss structure with sufficiently high natural frequencies, and then making tradeoffs between the natural frequencies of all structural components and the range, accuracy, and precision of the force measurements. To simplify the analyses, we assume that all these steps are decoupled, after which we highlight how the optimization of the natural frequency of the force plate and its support are strongly coupled. Finally, we give the mathematical equations used to analyze and design the AFP, as well as the details of the two AFPs presented, in the supplementary materials.
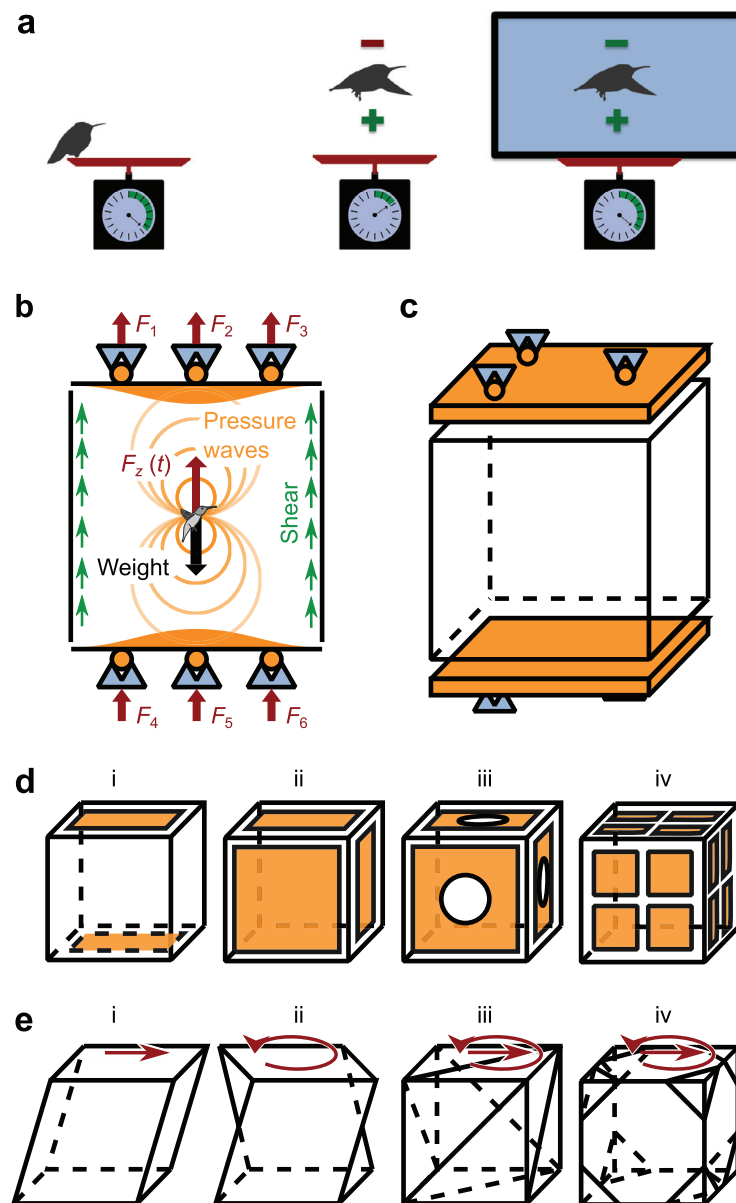
Figure 1. Working principle and setup of the aerodynamic force platform (AFP). (a) Simplified working principle: the vertical aerodynamic force supporting bodyweight originates primarily from a higher pressure $(+)$ below and a lower pressure $(-)$ above the bird. The higher pressure deflects the scale downward, which supports a fraction of body weight, but the lower pressure evades measurement (middle). By enclosing the bird with a physical control volume (blue box), the positive pressure can push down and the lower pressure can suck down the walls connected to the force sensor(s). (b) The bird generates a 3D unsteady aerodynamic force, of which we only show the vertical component, F_z, supporting bodyweight, W. This force is transferred via pressure waves as a pressure force normal and a small shear force tangential to the walls of the platform (Lentink *et al* 2015). Each wall transfers the aerodynamic load that acts on it to three statically determined contact points, with reaction forces $F_1 + F_2 + F_3$ on the top plate and $F_4 + F_5 + F_6$ on the bottom plate. (c) To integrate vertical aerodynamic weight support, instrumented force plates on the top and bottom are sufficient. Shear force is negligible and the sides can thus be closed with acrylic walls. (d) Whereas pressure force acting in one direction can be measured with two opposing panels (i), recording 3D force requires plates on all sides (ii). Adding acrylic windows enables optical access to the flight arena (iii). By constructing an array of $N \times N$ plates on all sides, with $N = 2$ shown, the pressure distributions can be measured (iv). (e) Simple frames supporting the plates are unable to resist shear (i) or torsion (ii) loads (red arrows) and thus vibrate at low frequency. Cross beams enable the structure to resist these loads with minimal deformation (iii), and corner cross beams improve access to the inner chamber (iv). The support truss rests in a statically determined manner on the ground with contact points that attenuate ground vibration.

Chamber size considerations

The airspace must be large enough to allow animals to behave naturally while small enough to give the AFP sufficient accuracy and precision. Although wall effects restrict airflow (Barlow *et al* 1999), our AFP flight volumes are comparable to those of wind tunnels for animal flight, and thus possess similar low levels of interference. For example, in the hummingbird setup, the ratio of chamber width (50 cm) to wingspan (12 cm) is 4.2, which limits wall effects on aerodynamic power to around 9% (Rayner 1991). Additionally, the ratio of the half-height of the chamber (25 cm) to wing radius (5.2 cm) is 4.8 such that the ground effect response on aerodynamic power is around 1% (Kim

et al 2014). Although the power required to fly in a confined chamber or test section may be somewhat less than what is required in open space (due to wall and ground effects), the force measured by the AFP is the actual aerodynamic force generated to fly in it (Lentink *et al* 2015). Further, our quadcopter studies show that accuracy is not affected by vortex wakes contacting the platform, as the unsteady and convective components are converted into unsteady pressure and shear stresses at the surface of the AFP (Lentink *et al* (2015), see Chu *et al* (1995) for vortex dynamics details). Larger chamber sizes offer more behavioral freedom at the cost of longer time delays because pressure waves, traveling at the speed of sound (figure S3), take longer to reach the instrumented force plates. In our new AFPs, the phase delay for a hummingbird hovering in the middle of the flight arena is 3.0% of the wingbeat period (wingbeat period, 24 ms; phase delay, 0.73 ms) and 2.6% of the wingbeat for a parrotlet flying in the middle of the flight arena (wingbeat period, 50 ms; phase delay, 1.3 ms). If only quasi-steady or time-averaged forces are of interest, the setup can be enlarged and supported by slower sensors.

Support truss vibration frequencies

To obtain time-resolved force measurements, the flight chamber and support structure must have natural frequencies that are much higher than the frequency content of the force generated by the locomoting animal or robot. Simple rectangular trusses lacking cross supports are relatively easy to deform through shear, torsion (figure 1(e) (i) and (ii)), and differential bending, where the torque is carried mainly in the form of transverse shear. These deformations correspond to much lower vibrational frequencies than those of the individual beam elements. Therefore, it is essential to use cross beams to suppress these lower frequency modes by enforcing additional 'fixed' boundary conditions along each beam (Chopra 1995). This can be achieved with full cross beams (figure 1(e) (iii)) or corner cross beams that increase access to the flight chamber (figure 1(e) (iv)).

Force plate support and chamber vibration frequencies

In addition to the truss supports, the frequency response of the AFP also depends on the force plate support and the flight chamber size. Similar to terrestrial force platforms (Biewener and Full 1992), all structural components should have natural frequencies that are much higher than the wingbeat frequency, f_{wingbeat}. However, higher natural frequencies require smaller dimensions and thus smaller flight volumes, so we recommend natural frequencies of about five times f_{wingbeat} or greater to maximize the flight volume while maintaining measurement fidelity. The natural frequency of the support is determined by mass load, m, and combined spring constant of the sensors, k (Chopra 1995):

$$f_{\text{support}} = \frac{1}{2\pi}\sqrt{\frac{k}{m}} \geq 5f_{\text{wingbeat}}. \tag{1}$$

This shows that plate mass should be minimized and sensor stiffness maximized. Carbon fiber sandwich panels can be used to limit plate mass. The maximum sensor stiffness is constrained by the resolution required to resolve the aerodynamic forces, which scale with animal or robot weight. For example, for a Pacific parrotlet (*Forpus coelestis*, approximate wingspan 20 cm, body mass 28 g, and wingbeat frequency 20 Hz) in the AFP for larger birds (total plate mass of 2132 g, see table S1), the minimum required equivalent stiffness for all three sensors according to equation (1) is about 840 kN m^{-1}. This resolution determines the minimum deformation or displacement needed for strain-based sensors (e.g. semiconductor strain gauges) or displacement-based sensors (e.g. capacitive or interferometry).

The natural reverberation frequency of the chamber depends on the x, y, and z lengths of the chamber, L_x, L_y, and L_z, and the speed of sound, c (Kleiner and Tichy 2014):

$$f_{\text{chamber}} = \frac{c}{2}\sqrt{\left(\frac{l}{L_x}\right)^2 + \left(\frac{m}{L_y}\right)^2 + \left(\frac{n}{L_z}\right)^2} \geq 5f_{\text{wingbeat}} \tag{2}$$

with acoustic mode numbers l, m, and n. The lowest (first) frequency mode is associated with the direction of the chamber that has the longest length. However, because we only need to consider directions in which force is being measured, for our vertical force platform (figure 1(b)) the first relevant mode is $l = 0$, $m = 0$, and $n = 1$, simplifying equation (2) as follows:

$$f_{\text{chamber}} = \frac{c}{2L_z} \geq 5f_{\text{wingbeat}}. \tag{3}$$

The maximum acceptable natural frequency determines the allowable chamber height. Keeping the natural frequencies of the chamber and support system about five times higher than f_{wingbeat} also prevents coupling phenomena between the chamber and support system, as shown in the resonance contour plot in figure 2(a). We determined this from a 1D acoustic fluid-structure interaction model (Lefrançois and Boufflet 2010; solved in MATLAB R2013a) in which we assumed that the plate is infinitely stiff and thus decoupled from the support structure frequencies.

Coupled force plate and support vibration frequencies

The force plates have complex vibration modes that depend on the carbon fiber layup (figure S5), materials, window design, location of the supports, and loading condition. The lowest frequency mode of a plate with isotropic face sheets (Leissa 1969) can be calculated as:

$$f_{\text{plate}} = \frac{B}{2\pi}\frac{h}{L^2}\sqrt{\frac{E_f t_f}{2\rho_{\text{area}}}} \geq 5f_{\text{wingbeat}} \tag{4}$$
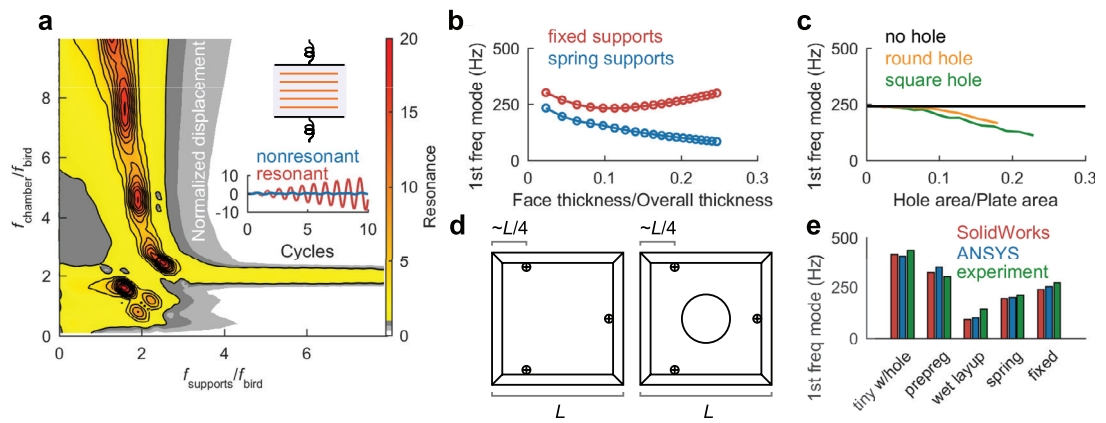
Figure 2. Structural optimization of the force plate and its support. (a) We created a 1D model of the AFP (inset), modeling the sensor supports and force plates as simple spring-mass systems. Resonance is measured by driving one of the plates with a sinusoidal motion at a distance of half the chamber height above the other plate, and measuring the amplitude response of the free plate over 50 cycles. For a resonant response, the normalized displacement grows in time, whereas a nonresonant response will remain stable with small amplitude (inset). This explains why resonance occurs at even multiples of the normalized natural frequency of the chamber. The resonance of the system is shown as a function of the natural frequencies of the chamber and the supports due to coupling by acoustic waves traveling between both plates. (b) For plates on fixed supports, increasing face sheet thickness increases the first natural frequency mode after a certain point. In contrast, for plates on spring supports the first natural frequency mode reduces monotonically. (c) For plates with windows, increasing the window size decreases the first natural frequency mode, but the reduction is minor for remarkably large holes. (d) Viewed from the bottom, the optimal location for the sensors is as close to the edges as feasible, both for a solid plate and a plate with a window. This also happens to match the configuration where all the sensors are spaced such that they are equally preloaded by the weight of the plate (figure S2). (e) ANSYS and SolidWorks FEM simulations agree well with experimental measurement of the lowest natural frequency for a range of force plate designs including: a 40×40 cm plate with a 12.5 cm diameter round hole, carbon fiber fabric that has been pre-impregnated with epoxy resin (prepreg), a wet layup in which the epoxy resin is impregnated by hand, and a plate tested on spring versus fixed supports. The carbon fiber plates are further described in table S1.

where the constant B is about 13 for the free boundary conditions of the AFP plate and a Poisson's ratio of 0.343 (comparable to most carbon fibers at 0.3), h the overall thickness of the sandwich panel, L is the longest length of the panel, t_f is the thickness of the face material (we assume $t_f \ll h$), E_f is the Young's modulus of the face material, and ρ_{area} is the overall mass density per unit area of the composite panel (ρ_{area} depends on face density of the carbon fiber ρ_f, thickness t_f and core density of the honeycomb ρ_c, as $\rho_{area} = 2\rho_f t_f + \rho_c(h - 2t_f)$). This equation assumes isotropic face sheets, but can be used to approximate the first frequency mode for orthotropic carbon fiber plates. For instance, for our hummingbird AFP force plates, we used a high-modulus carbon fiber face material (KVE Toray M55J) and low-density Nomex core material (Hexcel HRH-10 3 pcf 1/8″ cell). The plate frequency, f_{plate}, can be maximized most effectively by increasing panel height, h, relative to the panel length required for the chamber. Force plate optimization is strongly coupled with sensor support stiffness (figure 2(b)) which we evaluated using finite element method (FEM) analyses in SolidWorks (version 2014–2015). Due to this coupling, increasing t_f monotonically reduces f_{plate} when spring supports are used, contrary to what equation (4) suggests.

Panel window optimization

Optical and physical access to the AFP is necessary for camera recording of kinematics. Round windows yield higher natural frequencies than rectangular holes (based on FEM analyses in SolidWorks). If rectangular access is needed, rounded edges can mitigate the stress concentrations that would result from sharp corners (Pilkey and Pilkey 2008). Our simulations also show that round windows with an area of about 10% of the size of the plate lower the natural frequency by only 10% (figure 2(c)).

Support location optimization

Finally, we determine the best location for mounting supports on the plate to both maximize its natural frequency and preload all three sensors equally. Three contact points, each constraining two degrees of freedom, lock the plate into position in a statically determined manner, preventing thermal stresses and complex calibration routines. The simplest way to implement this support system is to rigidly connect the plate to three spherical surfaces, each of which rests on a vee-block (Bal-tec, VB-375-SM) fixed to a sensor. To preload all three sensors equally, one of the contact points should be located on the centerline (long axis) of the plate at distance l from the short axis, while the other two contact points should be located on opposite sides of the centerline, at a distance $l/2$ from the short axis. This equality in preloading also facilitates equivalent dynamic and aerodynamic loadbearing. We optimized these support locations through a batch FEM simulation (ANSYS 15.0) evaluating 200 different position combinations. The optimal configuration for a square plate of side length L has the contact point on the centerline $L/4$ from the center of
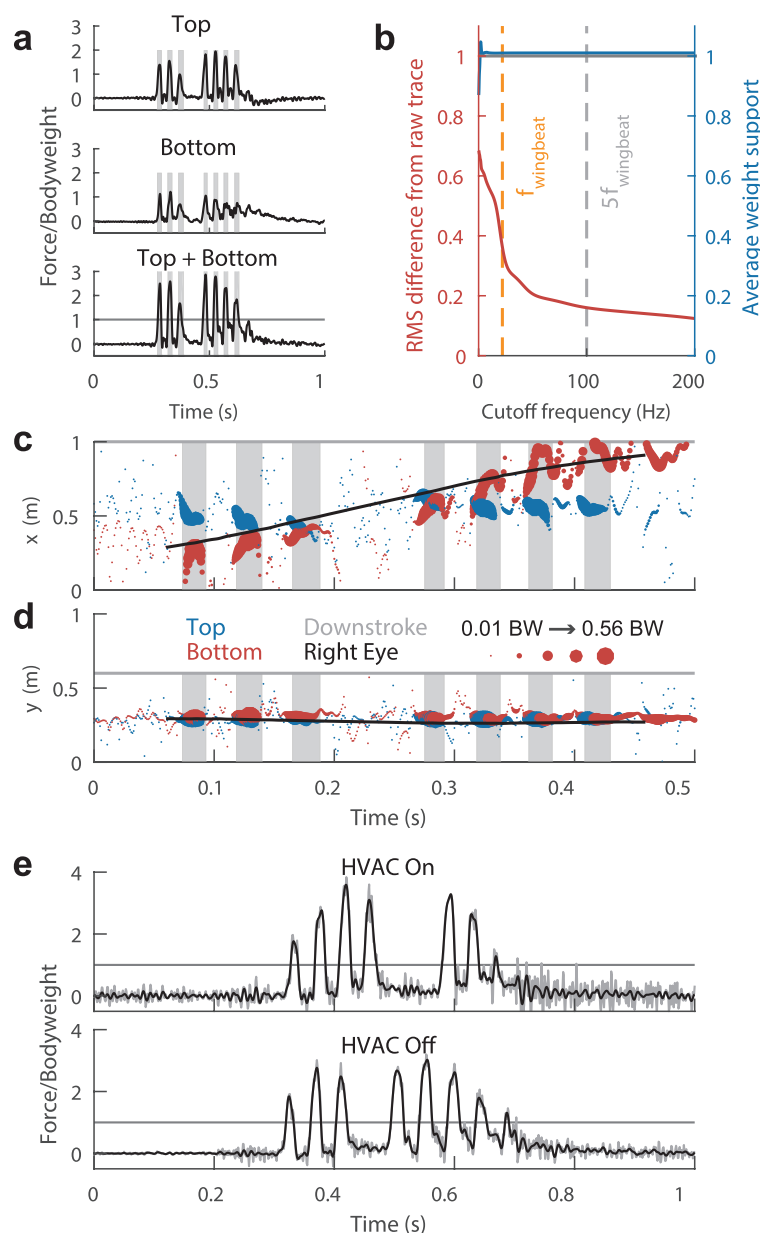
Figure 3. Aerodynamic force platform recording, accuracy and noise attenuation. (a) Aerodynamic force measurements of a Pacific parrotlet flying between two instrumented perches at 0.75 m distance in the AFP for larger birds (plate size 1.0×0.6 m). Both the top and bottom plate integrate the substantial pressure difference generated by the bird's wings (gray area, downstroke). While the instantaneous weight support changes, the average weight support over the flight should equal unity (grey line in bottom panel denotes weight support). (b) Low-pass filtering with cutoff frequencies about five times the wingbeat frequency preserves the accuracy of time-averaged bodyweight support measured by the AFP (instrumented perch data included). (c) and (d) The center of pressure on the aerodynamic force plate, in the flight (x) versus transverse (y) direction, progresses with the location of the bird's head (black). The location of the center of pressure becomes uncertain for low forces, when noise dominates the force differences between the three sensors on each plate (shown by making circle diameter proportional to force magnitude). (e) Recordings with HVAC on versus off. Raw data is in grey while filtered data is in black, and the grey line denotes weight support. Minimal infrasound improves the signal to noise ratio of the AFP.

the plate, whereas the other two contact points should be close to the opposite edge of the plate. This matches the configuration where the sensors are equally preloaded by the weight of the plate (figure 2(d)).

Finite element model simulations match experiment

Initially we performed FEM-based simulations using ANSYS to predict the performance of the plates. To validate the simulations, we compared the predicted first natural frequency modes with measured values obtained using a seismic accelerometer (Wilcoxon 731-207) connected to a handheld analyzer (Brüel and Kjær 2270) to acquire the data by exciting the plate with a light carbon fiber rod (figure 2(e)). The good correspondence, even when we made geometric simplifications by not including edge chamfers, inspired us to compare our results with basic SolidWorks FEM simulations. The results show that this commercial tool is not only useful for designing

the AFP, but also sufficiently accurate (figure 2(e)) for mechanical optimization of the force plates.

AFP force recording and noise mitigation

The net aerodynamic force is calculated by vectorially adding the forces integrated by each force plate. To ensure the aerodynamic force recordings are not only accurate, but also precise, ground vibrations and HVAC infrasound sources need to be identified, attenuated, and filtered out. We illustrate this for the large AFP with a Pacific parrotlet flying between perches across a horizontal distance of 75 cm. Figure 3(a) shows how the net vertical force is obtained from the individual contributions of the top and bottom plates. To check the accuracy of this setup and how this is modified by low-pass filtering the force, we calculate the average weight support across the flight (figure 3(b); this necessarily includes vertical forces generated by legs during take-off and landing, reported in Chin and Lentink, 2017). The AFP accurately records that the average vertical aerodynamic force is equal to weight (despite the lack of sidewall instrumentation; see Lentink *et al* (2015)). When the signal is low-pass filtered at five times the wingbeat frequency or faster, the weight support is close to unity (1.01 ± 0.04 for $N = 4$ birds making $n = 5$ level flights over 75 cm). Further increasing the cutoff frequency does not significantly affect the RMS difference from the raw trace (figure 3(b)). We expect similar results to hold for filtering measured forces generated by other flapping animals or robots because noise will dominate the signal at frequencies beyond five times the wingbeat frequency. The force generated in a hummingbird's wingbeat is mostly composed of frequencies at the flapping frequency and twice that due to the nature of the downstroke and upstroke both generating a pressure pulse. The center at which pressure acts on each plate (figures 3(c) and (d)) can be derived through a moment balance by using the positions of the three supporting sensors and the forces measured by each sensor. This location is precisely determined when force is high (downstroke) and imprecisely when force is close to the noise level (upstroke), despite the precision in the force recording itself throughout the stroke (figure 3(a)).

We used a Brüel and Kjær handheld analyzer with seismometer and infrasound (Brüel and Kjær 4964) probes to scout low vibration and low infrasound lab spaces and outdoor locations. Vibration isolation can be accomplished with simple dampers (Ruzicka and Derby 1971) or more advanced attenuation solutions (Doebelin 2010). For our setups, we found that simple vibration isolating leveling feet (Mighty Mount heavy duty vibration mounts) worked well. Infrasound-induced noise is easy to underestimate because the human ear is insensitive to the associated frequencies. Building codes allow HVAC units to produce high dB noise levels at low frequencies of around 5 Hz. Attenuating infrasound is infeasible given its long wavelength,

so HVACs should be turned off during recordings whenever possible. In contrast, the larger AFP for generalist birds can operate with HVAC on because the aerodynamic forces generated by these birds are significantly larger than HVAC noise (approaching peak forces of 1 N for parrotlets, figure 3(e)). If attenuation is insufficient, high frequency excitation responses of the AFP can be mitigated by low-pass filtering the force recordings at a cut-off frequency just below the noise excitation frequency. In addition, AC electromagnetic field frequencies might need to be filtered out with a 50 or 60 Hz notch-filter, depending on the country.

AFP leakage minimization using saran wrap

Due to design tolerances of the force plates, there may be small air leaks between the edges of the plates and sidewalls. These leaks may allow momentum to escape and connect the inside and outside (atmospheric) pressure fields, as in infrasonic microphones (Doebelin 2010). Previously we found that a large gap in the sidewall of our first-generation AFP did not significantly affect force measurement in the vertical direction (Lentink *et al* 2015), showing that leak-related filtering works differently in the AFP than modelled in infrasound microphones (Doebelin 2010). We found that gaps around the plate edges can filter the slowest aerodynamic force fluctuations measured by the plate. These gap effects may be more prevalent around the bottom plate, on which a net jet impinges during the free flight of an animal or robot. We found that leakage and the associated force filtering can be mitigated sufficiently by using saran wrap to loosely cover small gaps around the plates. Critically, saran wrap offers sufficient leakage resistance while its stiffness is low enough to avoid mechanical coupling between plates and the rest of the setup.

Conclusion

AFPs can be designed to be stiff yet lightweight so the natural frequencies of each component are at least five times higher than the frequency of interest. This results in high-frequency noise that can be filtered out to obtain accurate and precise measurements of aerodynamic force *in vivo*, as demonstrated here for a small generalist bird. We showed why it is essential to carefully consider the design of the support truss, force plates, windows, contact points, force sensor choice, and noise attenuation. Based on the design principles presented here and the theory published by Lentink *et al* (2015), the mechanical design of second-generation and future AFPs is straightforward with modern FEM software. The unique instrument can be used to directly record fluid mechanic forces for animals and robots in a much wider range of fluid media than presented here for air; its use for applications in biology, engineering and physics can be realized by complementing the principles introduced here with specific design constraints and commercial

multi-physics simulation software. Notwithstanding the broad range of applications, the immediate opportunity to perform high-throughput, real-time, non-intrusive, and *in vivo* comparative biomechanics analysis of force generation by locomoting animals—including aquatic, aerial, and bimodal terrestrial-aerial behaviors—will help advance the field of experimental biology and bioinspired design.

Competing interests

The authors declare no competing or financial interests.

Author contributions

BJH performed fluid simulations and drafted the manuscript. RI and DDC performed the experiments with hummingbirds and parrotlets respectively, and carried out data collection and analysis. RI and AFH built and characterized the hummingbird and larger bird AFPs, and CL built and analyzed the carbon fiber plates. DL developed the initial design principles behind the AFP and oversaw the project. All authors critically read and edited the manuscript.

References

Barlow J B, Rae W H and Pope A 1999 *Low-Speed Wind Tunnel Testing* 3rd edn (New York: Wiley)

Biewener A A and Full R J 1992 Force platform and kinematic analysis *Biomechanics: Structures and Systems: a Practical Approach* ed A Biewener (Oxford: Oxford University Press) pp 45–73

Chin D D and Lentink D 2016 Flapping wing aerodynamics: from insects to vertebrates *J. Exp. Biol.* **219** 920–32

Chin D D and Lentink D 2017 How birds direct impulse to minimize the energetic cost of foraging flight *Sci. Adv.* **3** e1603041

Chopra A K 1995 *Dynamics of Structures* vol 3 (Englewood Cliffs, NJ: Prentice Hall) p 339

Chu C C, Wang C T and Chang C C 1995 A vortex ring impinging on a solid plane surface—vortex structure and surface force *Phys. Fluids* **7** 1391–401

Doebelin E O 2010 *Instrumentation Design Studies* (Boca Raton, FL: CRC Press) https://doi.org/10.1201/9781439819487

Gutierrez E, Quinn D B, Chin D D and Lentink D 2016 Lift calculations based on accepted wake models for animal flight

are inconsistent and sensitive to vortex dynamics *Bioinspir. Biomim.* **12** 016004

Hedenström A, Van Griethuijsen L, Rosén M and Spedding G R 2006 Vortex wakes of birds: recent developments using digital particle image velocimetry in a wind tunnel *Animal Biol.* **56** 535–49

Johansson L C and Hedenström A 2009 The vortex wake of blackcaps (Sylvia atricapilla L.) measured using high-speed digital particle image velocimetry (DPIV) *J. Exp. Biol.* **212** 3365–76

Keennon M, Klingebiel K and Won H 2012 Development of the nano hummingbird: A tailless flapping wing micro air vehicle *50th AIAA Aerospace Sciences Meeting including the New Horizons Forum and Aerospace Exposition* https://doi.org/10.2514/6.2012-588

Kim E J, Wolf M, Ortega-Jimenez V M, Cheng S H and Dudley R 2014 Hovering performance of Anna's hummingbirds (*Calypte anna*) in ground effect *J. R. Soc. Interface* **11** 20140505

Kleiner M and Tichy J 2014 *Acoustics of Small Rooms* (Boca Raton, FL: CRC Press) https://doi.org/10.1201/b16866

Lefrançois E and Boufflet J P 2010 An introduction to fluid-structure interaction: application to the piston problem *SIAM Rev.* **52** 747–67

Leissa A W 1969 *Vibration of Plates* (Columbus, OH: Ohio State University)

Lentink D, Haselsteiner A F and Ingersoll R 2015 *In vivo* recording of aerodynamic force with an aerodynamic force platform: from drones to birds *J. R. Soc. Interface* **12** 20141283

Lentink D, Stefan R and Bradshaw N 2009 The scalable design of flapping micro-air vehicles inspired by insect flight *Flying Insects and Robots* (Berlin: Springer) https://doi.org/10.1007/978-3-540-89393-6_14

Ma K Y, Chirarattananon P and Fuller S B 2013 Controlled flight of a biologically inspired, insect-scale robot *Science* **340** 603–7

Mohebbian A and Rival D E 2012 Assessment of the derivative-moment transformation method for unsteady-load estimation *Exp. Fluids* **53** 319–30

Muijres F T, Spedding G R, Winter Y and Hedenström A 2011 Actuator disk model and span efficiency of flapping flight in bats based on time-resolved PIV measurements *Exp. Fluids* **51** 511–25

Noca F, Shiels D and Jeon D 1999 A comparison of methods for evaluating time-dependent fluid dynamic forces on bodies, using only velocity fields and their derivatives *J. Fluids Struct.* **13** 551–78

Pilkey W D and Pilkey D F 2008 *Peterson's Stress Concentration Factors* (New York: Wiley)

Ramezani A, Chung S and Hutchinson S 2017 A biomimetic robotic platform to study flight specializations of bats *Sci. Robot.* **2** eaal2505

Rayner J M and Thomas A L 1991 On the vortex wake of an animal flying in a confined volume *Phil. Trans. R. Soc.* B **334** 107–17

Rival D E and Van Oudheusden B W 2017 Load-estimation techniques for unsteady incompressible flows *Exp. Fluids* **58** 20

Ruzicka J E and Derby T F 1971 *Influence of Damping in Vibration Isolation* (Washington, DC: US Department of Defense) ch 7

Shyy W, Aono H, Kang C K and Liu H 2013 *An Introduction to Flapping Wing Aerodynamics* vol 37 (Cambridge: Cambridge University Press) https://doi.org/10.1017/CBO9781139583916

Taylor G K 2001 Mechanics and aerodynamics of insect flight control *Biol. Rev.* **76** 449–71

Van Oudheusden B W 2013 PIV-based pressure measurement *Meas. Sci. Technol.* **24** 032001

Zhao L, Huang Q, Deng X and Sane S P 2010 Aerodynamic effects of flexibility in flapping wings *J. R. Soc. Interface* **7** 485–97